PCCP

Accepted Manuscript




ROYAL SOCIETY OF CHEMISTRY

www.rsc.org/pccp

# A Simple Model of Burst Nucleation

Alexandr Baronov, Kevin Bufkin, Dan W. Shaw, Brad L. Johnson, David L. Patrick
*Advanced Materials Science and Engineering Center,*
*Western Washington University, Bellingham, WA 98225*

We introduce a comprehensive quantitative treatment for burst nucleation (BN), a kinetic pathway toward self-assembly or crystallization defined by an extended post-supersaturation induction period, followed by a burst of nucleation, and finally the growth of existing stable assemblages absent the formation of new ones, based on a hybrid mean field rate equation model incorporating thermodynamic treatment of the saturated solvent from classical nucleation theory. A key element is the incorporation of a concentration-dependent critical nucleus size, determined self-consistently along with the various subcritical cluster population densities. The model is applied to an example experimental study of crystallization in tetracene films prepared by organic vapor-liquid-solid deposition, where good agreement is observed with several aspects of the experiment using a single, physically well-defined adjustable parameter. The model predicts many important features of the experiment, and can be generalized to describe other self-organizing systems exhibiting BN kinetics.

PACS numbers: 68.55.A-, 81.05.Fb, 81.10.Aj, 81.15.Aa

Many self-organizing systems provided with an ongoing supply of fresh growth units are found to undergo burst nucleation (BN), characterized by an extensive post-supersaturation induction time, followed by a transient burst of nucleation, then continued growth of existing nuclei absent the formation of many new ones. BN has been observed in situations as diverse as setting concrete[1], infection-induced cellular lysis[2], the preparation of synthetic nanoparticles[3, 4], and vapor-liquid-solid deposition.[5, 6] In systems exhibiting BN kinetics, nucleation and growth are separated in time, and hence can be performed under different experimental conditions; this distinguishes BN from other modes of monomer aggregation[7], and can be exploited, for example, to produce nanostructures incorporating heterointerfaces.[8] Since nucleation is limited to a relatively short period of time, BN is perhaps the most widely invoked mechanism for understanding size distributions in the preparation of monodisperse nanoparticles.[9–11]

The underlying mechanisms responsible for BN may be varied, and system-dependent. For example, in a closed system containing a finite number of heterogeneous nucleation sites, such as foreign particles, heterogeneous nucleation may be transitory, lasting only until all such sites have been titrated by nuclei.[12] In systems subjected to mechanical agitation, so-called secondary nucleation can result from the growth of daughter fragments detached from parent crystals, a mechanism which can lead to a rapid but brief increase in the apparent nucleation rate.[13, 14] Another mechanism, proposed for certain metal nanoparticle syntheses,[15] postulates a two-step process combining slow, continuous nucleation with fast autocatalytic surface growth. The large difference in rate constants for the two steps leads to BN.[16]

In contrast, here we are interested in homogeneous nucleation within a system fed by a continuous supply of fresh monomers with negligible heterogeneous or secondary nucleation, perhaps the simplest situation producing BN behavior. Such a scenario was originally studied by LaMer and Denegar (LD)[17], whose classic explanation for BN kinetics remains by far the most widely cited and studied one. LD postulated a time-dependent rise and fall of the monomer concentration $n$, where a flux $F$ of new monomers is continuously provided from an external reservoir: $F(t) > 0$. The main features of the LD picture are illustrated in Figure (1). During the induction regime $n$ increases as a result of the flux, rising until a critical supersaturation $n^*$ is reached and crystallization commences. Drivers of $n$ can include the chemical decomposition of monomer-generating precursors in solution as studied originally by LaMer and Dinegar, the flux of growth units from the vapor onto a surface as studied here, or a continuous change of temperature in a closed system, such as in a batch crystallizer, where

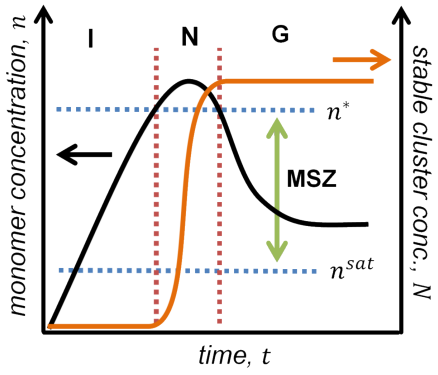


FIG. 1. The LaMer-Dinegar model of delayed burst nucleation. I = induction regime, N = nucleation regime, G = growth regime. $n^*$ and $n^{sat}$ are the monomer concentrations where nucleation begins and at saturation, respectively. MSZ is the metastable zone where growth of existing stable clusters, absent nucleation, occurs. (Color online)

it is the monomer chemical potential, rather than con-

centration, that is driven. The formation and growth of stable nuclei in the subsequent nucleation regime rapidly outstrips the flux, depleting the monomer concentration until a steady-state condition within the metastable zone $n^{sat} \leq n \leq n^*$ is reached, where $n^{sat}$ is the monomer concentration at saturation; this halts further nucleation but permits growth of existing nuclei. The LD model applies to early-stage growth, excluding coarsening processes such as Ostwald ripening or further aggregation among supercritical clusters.[18]

Despite its important role in understanding the origins of BN in a wide range of systems, few quantitative formulations of the LD mechanism have been proposed, and direct comparison to experiments under unambiguous LD conditions are rare.[19] Recently, Privman and coworkers introduced a model combining classical nucleation theory (CNT) with a rate equation treatment for monomer and supercritical cluster aggregation to study burst nucleation and cluster size distributions in the formation of monodisperse colloids.[20, 21] However, the model begins with a large supersaturation, masking details of the induction regime, and the total number of monomers in the system is conserved, i.e. $F(t) = 0$.

In this paper we introduce a semi-empirical hybrid kinetic-thermodynamic approach to modeling BN under LD conditions ($F(t) > 0$, and no subsequent coarsening processes) wherein a traditional rate equation structure is modified to include the effects of cluster surface energy and monomer concentration in dynamically determining the critical nucleus size and also explicitly incorporating the rates for attachment and detachment of subcritical clusters via exchange with a surrounding solvent. The purpose is to provide a simple, effective quantitative description of BN that explicitly elucidates the key global mechanisms applicable to a range of systems and growth habits (i.e. independent of crystal shape/morphology and diffusion-, reaction-, or attachment-limited growth kinetics; these details can be included in the present model, but we focus instead on the foundational elements of BN[22]).

The key new feature of the present treatment is the self-consistent incorporation of a monomer-concentration-dependent critical nucleus size. We demonstrate that the critical size plays a catalytic role, activating the nucleation mechanism (explicitly governed by the coupled rate equations), and after nucleation is initiated, the subsequent reduction of monomer concentration causes the critical size to abruptly increase, terminating nucleation on short time scales. As formulated, the model is the simplest embodiment of the LD theory capturing all microscopic processes, and the first quantitative model of the full LD mechanism. It reduces exactly to a standard mean field rate equation (MFRE) model in the (fixed) small critical nucleus size limit but produces good agreement with classical nucleation theory (CNT) in the prediction of the critical nucleus size, thereby bridging the two paradigmatic frameworks. We apply our model to analyze early stage nucleation and growth in tetracene films prepared by organic vapor-liquid-solid (VLS) deposition, under conditions wherein Ostwald ripening and supercritical cluster aggregation are both negligible, producing archetypal LD kinetics. We find good quantitative agreement using a single, physically well-defined adjustable parameter.

The proposed model is constructed around a simplified MFRE set incorporating terms accounting for the elementary processes of monomer flux, diffusion, and aggregation.[23, 24] The treatment is limited to two bulk populations:[25, 26] the concentration of sub-critical clusters $n$, which is dominated by monomers, and supercritical (thermodynamically stable) clusters $N$[27]. The two-population approximation reduces the model to the simplest components capable of encompassing the essential mechanisms in a mathematically tractable and complete fashion–thermodynamically-driven critical nucleation and (mean-field) population dynamics. The kinetics of the two populations are governed by coupled rate equations, vis.

$$\frac{dn}{dt} = F - KP(i^*, n)n - KnN \quad (1)$$

$$\frac{dN}{dt} = KP(i^*, n)n \quad (2)$$

Here $K$ is a collision and capture kernel for diffusing species and $P(i^*, n)$ is the concentration of aggregates (at monomer concentration $n$) of size $i^*$, with $i^*$ defined as one monomer less than the critical stable cluster size. The mathematical forms of Equations (1) and (2) represent the processes of monomer addition, loss of subcritical clusters via the collision and capture of a monomer with/by a cluster of size $i^*$ (with a corresponding gain in the stable cluster density via the same process) and the loss of subcritical density via the collision (and possible capture) of sub-critical clusters with stable clusters. The capture of a monomer by a stable island is assumed irreversible. Most important, the connection of the kinetics to the thermodynamics is accounted for in the construction of the functions $K$ and $P$.

To construct the distribution $P(i^*, n)$ we begin with the free energy of a cluster of size $i$ at concentration $n$:[28–30]

$$\Delta G_i(n) = -(i-1)kT \ln\left(\frac{n}{n^{sat}}\right) + 4\pi\sigma a^2\left(i^{2/3} - 1\right) \quad (3)$$

Here $n^{sat}$ is the monomer equilibrium (saturation) concentration, $k$ is the Boltzmann constant, $T$ is the absolute temperature, $a$ is the monomer radius (assuming spherical monomers), and $\sigma$ is the cluster surface energy. The first term derives from the entropy of dispersed monomers in the solvent. The second term is the surface energy associated with the creation of a cluster of size $i$, which is assumed for the sake of simplicity to be spherical with a size-independent surface energy[31]. Assuming

rapid attachment/detachment kinetics, the concentration of sub-critical clusters is a thermalized distribution, vis. $P(i,n) = n \exp\left[\frac{-\Delta G_i(n)}{kT}\right]$ and therefore

$$P(i,n) = n\left(\frac{n}{n_o}\right)^{i-1} \exp\left[\frac{-4\pi\sigma a^2(i^{2/3}-1)}{kT}\right] \quad (4)$$

which then leads immediately to the relationship for $P(i^*,n)$ (Equation (4) has been constructed directly from the main ideas of CNT, and is closely related to the so-called Walton relation.[32] The difference, in this case, is centered around the monomer concentration-dependent parameter $i^*$, which is developed below).

We adopt the form of the collision kernel $K$ as a modified Smoluchowski function[33] for the rate of collision between diffusing monomers and spherical clusters of size $i^*$: $K \approx \gamma 4\pi a i^{*1/3} D$. Here $D$ is the monomer diffusion coefficient and $\gamma$ is the condensation coefficient, equal to the monomer capture probability given a collision has occurred. This (mean-field) parameter incorporates the microscopic rate constants governing the association and dissociation of monomers to and from the cluster surface.

Lastly, the critical size $i^*$ itself is determined via maximization of the free energy (3) with respect to cluster size, and in this case we find

$$i^*(n) = \left(\frac{8\pi\sigma a^2}{3kT\ln(n/n^{sat})}\right)^3 \quad (5)$$

The resulting model predicts the signature features of BN: In the initial stages of flux delivery, the monomer concentration is only slightly greater than the equilibrium concentration, and therefore $i^*$ is very large (see equation (5). Large $i^*$ leads to the condition $P(i^*,n) \approx 0$, and the rate equations reduce to $dN/dt \approx 0$, (no nucleation, and thus $N \approx 0$) and $dn/dt \approx F$, giving $n(t) = Ft$. Together these conditions describe the induction regime with its linear increase in monomer concentration. Similarly, as mentioned above, following nucleation of stable clusters the monomer concentration drops rapidly, as diffusing monomers are significantly more likely to encounter a stable cluster than to randomly aggregate into a cluster of size $i^* - 1$, and therefore the critical size will again increase sharply and inhibit the terms involving $P(i^*,n) \approx 0$, and nucleation ceases. Following nucleation, then, the stable cluster density is constant ($N = N_q$), and the rate equation for the subcritical density is given by $dn/dt \approx F - KN_q n$. If we make the simplifying assumption that the critical nucleus size is a large constant (large enough to warrant the approximation $P(i^*,n) \approx 0$), then $K = K_q$ (a constant), and the rate equation admits solutions given by

$$n(t) = \frac{F}{K_q N_q} + ce^{-K_q N_q t} \quad (6)$$

where $c$ is an integration constant. Equation (6) is the predicted form of the LD monomer curve in the growth regime, which asymptotically approaches $F/(K_q N_q)$ in the metastable zone.

We utilize the assumption that the size distribution of subcritical clusters is dominated by the monomers; this then assumes the formation/dissolution rate of subcritical clusters is high, and is supported by the form of the concentration distribution given by Equation (4). In addition, for $i^* = 1$, $P = n$ directly, in agreement with established MFRE models for $i^* = 1$.[26] Hence the rate equations (1) and (2) reduce to the familiar form for the irreversible deposition-diffusion-aggregation model in the limit $i^* = 1$, with modifications of the diffusion coefficient to include capture probability via the Smoluchowski equation.

We apply the model to study BN in the formation of $\mu m$-sized crystals of the organic semiconductor tetracene, grown in a solvent of bis(2-ethylhexyl)sebecate (BES). A steady rate of monomer addition was achieved by supplying growth units to a thin solvent layer from the vapor, which resulted in the formation of small crystals whose appearance and growth were quantified via direct, in-situ observation using videomicroscopy. The method is an all-organic analog to the vapor-liquid-solid (VLS) technique of crystal growth introduced by Wagner and Ellis for inorganic materials in liquid metal alloy droplets[34–37], but employs an organic[38–41], ionic liquid[42–44], or liquid crystalline[45] solvent combined with an organic precursor delivered via the vapor phase. As the solvent layer becomes saturated, crystals form in a quasi- two-dimensional liquid environment, but they tend to stay in fixed positions, similar to island growth on bare surfaces. Film formation thus combines elements of physical vapor deposition and solution-phase crystal growth.

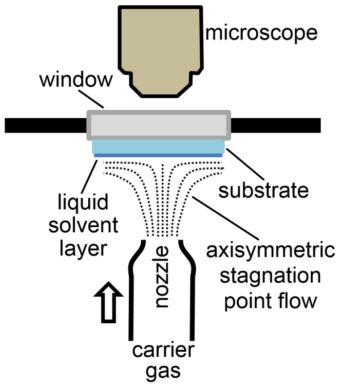


FIG. 2. Schematic of the experimental apparatus. Sublimate exited a heated source cell through a pinhole opening and was carried by a stream of $N_2$ out a tapered nozzle toward the substrate. A shutter between the nozzle and substrate (not shown) controlled deposition. Film growth was monitored in situ through a transparent window with polarized optical microscopy. The geometry of the impinging jet produces axisymmetric stagnation point flow. (Color online)

Tetracene vapor was deposited into a $1.9 \pm 0.3\mu m$

thick layer of BES spread onto a supporting Indium-Tin-oxide-coated (ITO) glass substrate. BES is a clear and colorless hydrophobic liquid with a low vapor pressure at room temperature and good spreading properties on ITO-coated glass. Solvent layer thickness was determined by interferometry. Deposition was performed in a sealed chamber under 1 atm. of $N_2$. Tetracene vapor generated in a heated crucible was swept into flowing nitrogen and directed at the substrate by a tapered nozzle, producing a laminar axisymmetric impinging flow giving nearly uniform deposition over an area $\approx 1cm^2$ in size (Figure 2). A movable shutter was used to start the experiment. The gas flow serves to enhance deposition efficiency by increasing mass transport across the static boundary layer at the gas-liquid interface. A tapered constriction at the nozzle's terminus flattened the velocity profile from Poiselle-like to plug-like flow, so that the variation in F over the analysis region was less than 10%. Videos of film growth were captured in situ with polarized optical microscopy. Further details are provided in Ref. [47].

Figure (3) presents micrographs showing the development of a tetracene film. Figure 3A, acquired $t = 5.3min$

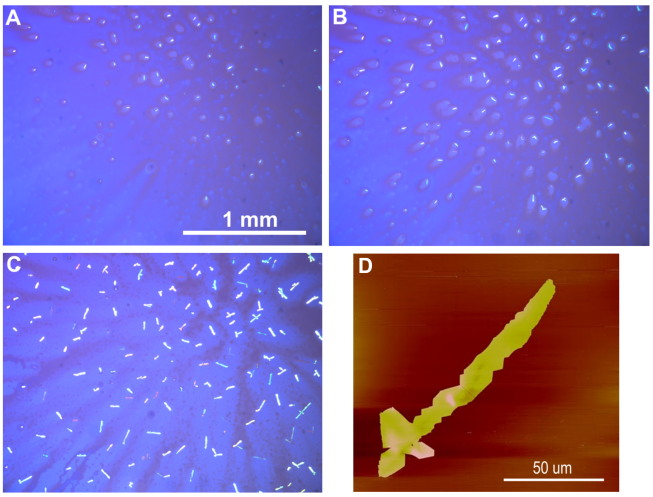


FIG. 3. (A-C) Polarized optical micrographs at various stages of film development. (A) $t = 5.3min.$ after the start of deposition, near the beginning of the nucleation regime; (B) $t = 6.8min.$, near the end of the nucleation regime; (C) $t = 16.3min.$, after nucleation had ceased and the growth regime was well established. (D) Atomic force microscopy image of a representative crystal. (Color online)

after the start of deposition, shows the beginning stages of nucleation, where each visible bright object eventually grows into a distinct crystal. Figures 3B and 3C correspond to the middle of the nucleation regime and the growth regime, respectively. Crystals were generally compact, with partially branched habits (Fig. 3D). Post-deposition high resolution polarized optical micrographs (Figure S4) demonstrate that each object in Figure 3 is a single monocrystal, and not an aggregate of smaller crystals. Growth was observed to be quasi-two dimensional, with lateral (in-plane) sizes approaching 100 m by the end of the analysis period, but crystal thickness, measured by atomic force microscopy after deposition was complete, being only $\approx 75nm$. This thickness was found to be about the same for all crystals measured, regardless of their size (Fig. S1). Crystals grew with random in-plane, but uniform out-of-plane orientation, with the (001) plane parallel to the liquid surface, as determined by x-ray diffraction (Fig. S2). Occasionally, very small crystals would be observed to move if the solvent layer was disturbed, but once they had grown to several tens of microns in size they became essentially immobile. This suggests that crystals were not initially attached to the substrate, i.e. growth did not initiate with heterogeneous nucleation at the ITO/solvent interface. Crystals were also fully wetted by BES and therefore completely submerged in the solvent. Thus crystals appeared to form in the solvent, as free-floating nuclei. Once crystals had grown to a certain size, capillary forces would have pressed them against the substrate, making them immobile. Halting deposition by closing the shutter led to the cessation of growth without further changes in crystal size or shape over the timescale of the experiment. Over a period of many hours Ostwald ripening was observed to gradually occur, but the rate of this process appeared negligible on the timescale of the analysis. Together these results support the assumption that processes of supercritical cluster aggregation and coarsening can be neglected, leading to archetypal La Mer-Dinegar BN kinetics.

The time evolution of the crystal concentration $N(t)$ determined by counting the number of visible crystals per unit volume of solvent is shown in Figure 4A. Three distinct regimes may be identified: (i) An induction regime between the onset of deposition and the first appearance of crystals. Its duration depended on the deposition rate, being shorter for higher rates. It could also be made shorter (but not equal to zero) by using BES that was pre-saturated with tetracene[46] prior to the start of deposition, demonstrating that the solution had to become significantly supersaturated before crystals started to form. Since the smallest crystal which could be detected in the digital microscope images was $\approx 10\mu m^2$, and during the nucleation regime crystals grew in size at an average rate of $\approx 250\mu m^2 min^{-1}$, the induction time was essentially equivalent to the first appearance of crystals in the video images, which were acquired in 15 sec. intervals. (ii) The induction regime was followed by a nucleation regime during which new crystals formed and existing crystals grew. The peak nucleation rate occurred at $t = 8min.$ and dropped nearly to zero less than two minutes later. In terms of 2D coverage, the projected fractional surface area occupied by crystals was 0.006 at the peak nucleation rate, increasing to 0.03 by the time

nucleation ceased. Crystals were thus widely separated relative to their initial sizes, consistent with independent nucleation. (iii) The nucleation regime was followed by a growth regime during which crystals increased in size but no new crystals formed.

To enable quantitative comparison to the proposed model, the time evolution of both the stable crystal density and the tetracene concentration are required. The latter may be obtained as follows. Assuming uniform mixing,[48] the concentration $C(t) = \sum_{i=1}^{i^*} iP(i,n)$ of dissolved tetracene in the solvent layer is found from the mass balance between the integrated flux and the number of molecules incorporated into crystals:

$$C(t) = \int_0^t F dt - A(t) d_c \rho_c / d_s \qquad (7)$$

where $A(t)$ is the total crystal area per unit substrate area, $d_c$ is the crystal thickness, $d_s$ is the solvent thickness, and $\rho_c = 3.42 \times 10^{27} m^{-3}$ is the monomer number density of crystalline tetracene.[49] The volumetric flux $F$ was determined by matching the arrival rate of new tetracene from the gas phase with the incorporation rate of tetracene into growing crystals during the steady-state conditions occurring after nucleation had ceased and the growth regime was well established: $F = G d_c \rho_c / d_s$, where $G = dA/dt$ is the total areal crystal growth rate per unit substrate area (in $s^{-1}$) (in the present case, $G = 2.67 \times 10^{-5} s^{-1}$). Solvent layer and average crystal thickness were measured by interferometry and atomic force microscopy, respectively, and found to be $d_s = 1.9 \mu m$, and $d_c = 75 nm$ (Figure S1). This gave $F = 9.5 \times 10^{21} m^{-3} s^{-1}$. The monomer concentration computed in this way is plotted in Figure (4A) (filled circles) along with the resulting density of stable crystals (open circles).

Overlaid in Figure (4A) (solid lines) are the model results obtained by using parameters appropriate to the tetracene experiment, vis: $n_o = C^{sat}$, along with $a = 4.11 \times 10^{-10} m$,[49] $\sigma = 25 m J m^{-2}$,[50] and $D = kT/6\pi\epsilon a = 5.34 \times 10^{-11} m^2 s^{-1}$ ($\epsilon = 0.01 Pas$ is the solvent viscosity, $T = 300K$ is the temperature and $k$ is Boltzmann's constant). The only unknown parameter is the condensation coefficient, which was determined by simultaneously fitting the experimental results in Figure (4A) for both $n(t)$ and $N(t)$, giving $\gamma = 7 \times 10^{-8}$. This value of the condensation coefficient is reasonable, based on its mean-field kinematic role as averaging the stochastic rates of association and dissociation of clusters of all sizes (including stable islands, which also suffer dissociation, but have a net average growth). In the current application, nucleation and growth occur in a solvent solution, greatly narrowing the gap between the attachment and dissociation rate constants. When the rate constants for attachment ($k_a$) and dissociation ($k_d$) obey $k_a >> k_d$, the condensation coefficient is roughly equal to the areal growth of stable islands per time per area;

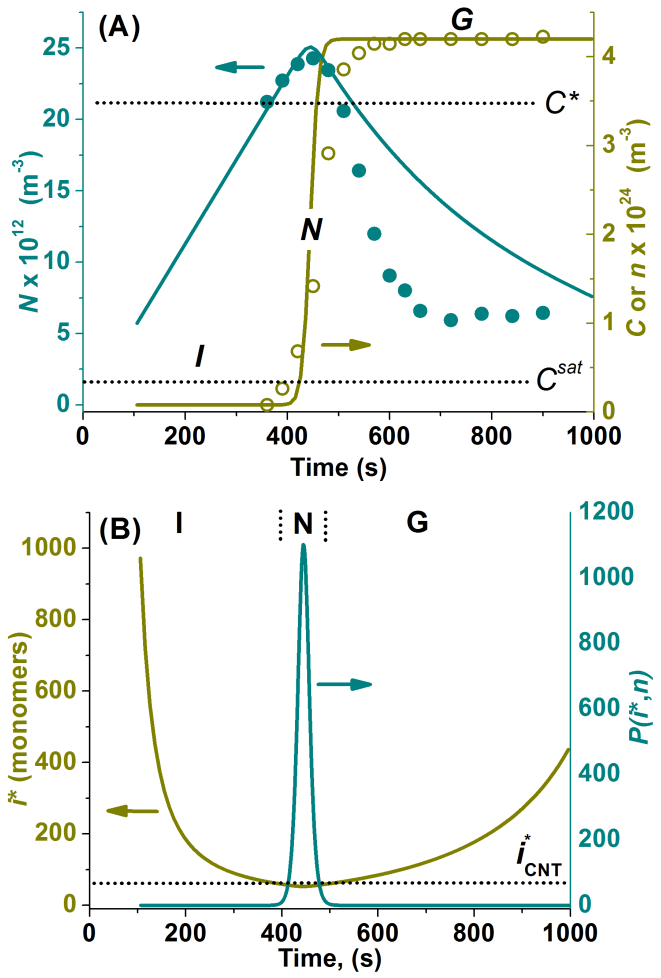


FIG. 4. (A) The concentration of precursors and stable crystals as a function of time since the onset of deposition. Open and solid points from experiment. Solid lines are model results (see text for parameters). (B) The model predictions for the critical nucleus size $i^*$ and the precursor distribution function $P(i^*, n)$. Note the demarkation of the nucleation regime corresponding to simultaneous minimum in $i^*$ and onset/peak/decline of $P(i^*, n)$. (Color online)

when dissociation rates are appreciable, as in the present case, the condensation coefficient is much smaller, as flux rates and precursor concentrations greatly exceed areal growth rates[51].

The model provides remarkable agreement with most aspects of the experiment, including the existence of the three signature regimes of BN, i.e. induction, nucleation, and growth regimes, a high monomer concentration relative to the stable cluster concentration ($n >> N$), as well as quantitative agreement in the nucleation onset time, peak monomer concentration, and concentration of stable clusters. The main discrepancy is an underestimation of the rate of decline in the monomer concentration at the beginning of the growth regime. We speculate this may be caused in part by shear thinning of the solvent layer

during deposition under the impinging gas flow. Solvent thinning-for a constant areal flux of monomers-results in a higher volumetric-flux rate and a corresponding larger monomer concentration in the experiment than would be computed from the relationship $C(t)$ above. The critical concentration (shown in Figure (4A)) is found to be $C^* = 3.6 \times 10^{24} m^{-3}$, and the critical supersaturation ratio $S^* = C^*/C^{sat} = 9$, based on the equilibrium saturation concentration $C^{sat} = (4.2 \pm 0.6) \times 10^{23} m^{-3}$, measured separately by UV-Vis absorption spectroscopy of a bulk equilibrated BES solution saturated in tetracence. The saturation ratio determined here is similar to that reported for VLS growth in some inorganic systems,[52] and further demonstrates that significant supersaturation is required for crystal nucleation to occur. The model prediction for $n^*$ via the value of $n(t)$ at the onset of nucleation gives $n^* = 3.8 \times 10^{24} m^{-3}$, in excellent agreement with the observed $C^*$.

The central significance of the model, and the primary result of this paper, is illuminated via self-consistent calculation of the critical size $i^\star$ over the course of the experiment. In Figure (4B), we show the model predictions for the critical nucleus size $i^*(t)$ and the corresponding distribution $P(i^*, n)$ for the parameters of the experiment. The important features of the model are evident: at the onset of deposition the monomer concentration is small, so $i^*$ is initially large. As the flux of new growth units from the vapor increases $n(t)$, $i^*$ decreases, reaching a minimum $i^*_N \approx 53$ in the nucleation regime. Nucleation occurs when the critical size decreases sufficiently such that the distribution function $P(i^*, n)$ becomes appreciable, triggering the coupling of equations (1) and (2), which is the mechanism for the initiation of nucleation. Thereafter monomers are increasingly consumed by growing crystals, causing $i^*$ to rise again, and further nucleation to cease. Also note in Figure (4B) that the function $P(i^*, n)$, which, as pointed out, becomes appreciable only in the nucleation regime, serves to define both the onset and terminus of the nucleation regime. Together these results highlight the importance of the changing critical nucleus size in producing BN behavior.

The value of $i^*_N$ given by the model can be compared to the critical nucleus size predicted from classical nucleation theory. For a spherical nucleus, the latter is given by $r_c = (8/3)\pi\sigma a^3/\Delta\mu^* = 1.63nm$, where the Gibbs potential energy difference $\Delta\mu^*$ between a monomer in solution at concentration $C^*$ and in the crystalline state is $\Delta\mu^* = kTln(C^*/C^{sat}) = 8.9 \times 10^{-21} J$ at $T = 300K$. This corresponds to $i^*_{CNT} = 62$ monomers, in good agreement with the value $i^*_N$ reported above.

In addition, the model rate equations may be employed to analyze the scaling of the equilibrium crystal density with the flux. It has been shown previously that two-component rate equation models with fixed $i^*$ predict that the equilibrium crystal density should scale with flux, according to $N(F) \approx F^\chi$, where $\chi = i^\star/(i^\star + 2)$[53].

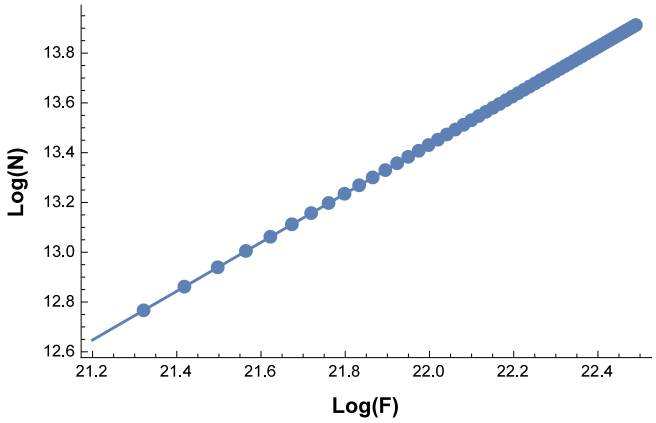


FIG. 5. The Log of the equilibrium crystal density vs. the Log of the volumetric flux as predicted by the model, utilizing parameters from the experimental fit of figure (4). The lines is a linear fit, giving a scaling exponent of 0.98.(Color online)

More recently, it has been shown that in the presence of an energy barrier inhibiting attachment of monomers at crystal edges, the scaling of crystal density with flux may be significantly altered, i.e. $\chi \approx 2i^*/(i^* + 3)$[54]. Therefore, in the limit of large $i^*$, the two predictions converge to $\chi \approx 1$ and $\chi \approx 2$, respectively. In order to compare the current model–which assumes an effective attachment barrier (small condensation coefficient, via appreciable attament/detachment rates)–we run a numerical experiment for the equilibrium crystal density as a function of flux, using the parameters from the tetracene/BES experiment as a baseline. Figure (5) shows the model prediction for the scaling of stable crystal density with flux. The plot depicts the Log of crystal density vs. the Log of the volumetric flux into the liquid solvent; the resulting linear fit indicates a scaling exponent of $\chi = 0.98$. If we adopt the critical nucleus size of $i^*_N = 53$ as above, we expect, in the absence of an attachment barrier, $\chi = 53/55 = 0.96$. The agreement would indicate that the rapid onset and rise of nucleation associated with BN, in the current model, compensates for the detachment rate effects of the solvent. It is worth noting that a similar numerical result for the scaling of the equilibrium crystal density with condensation coefficient predicts a scaling of $N \approx \gamma^{-0.98}$, or roughly inverse scaling–a surprising result[55]. Lastly, we note that model predicts a power-law scaling of the induction time with the condensation coefficient, vis. $t_{ind} \approx \gamma^{-0.035}$, such that long induction times are predicted when association and dissociation rate constants are comparable, resulting in a low probability of monomer sticking per collision.

In summary, we have studied the general phenomenon of burst nucleation within a unified thermodynamic/kinetic mean field rate equation framework, wherein the combined effects of a monomer driving source (here provided by a vapor-phase flux) and a solvent (forc-

ing the monomer concentration to significantly exceed the saturation concentration in order for nucleation to occur) modify the rate equations, giving qualitatively different nucleation and growth behavior relative to standard MFRE approaches. A key feature is the self-consistent inclusion of a monomer-concentration-dependent critical nucleus size, which controls the onset and duration of the nucleation regime by activating the monomer capture terms in the rate equations. This leads to a substantial induction regime, a sharply-defined nucleation regime followed by pure growth, as well as a large difference in the equilibrium monomer and stable-crystal concentrations. The model predicts a critical nucleus size consistent with classical nucleation theory, but reduces to the standard MFRE result in the limit $i^* = 1$. As the first comprehensive quantitative formulation of LD kinetics, we note the potential to extend the model to include different drivers of the monomer concentration, reaction- or diffusion-limited growth, and size- and shape-dependent surface energy.

This work was supported by the National Science Foundation (DMR-0705908 and DMR-1207338). The authors thank B. Ricker for his contributions.

[1] V. S. Ramachandran, *Concrete Admixtures Handbook Properties, Science, and Technology*, 2nd ed.; (Noyes Publications: Park Ridge, 1995).
[2] G. L. Ryan and A. J. Rutenberg, Bacteriol. **189**, 4749 (2007).
[3] J. Park, J. Joo, S. G. Kwon, Y. Jang, and T. Hyeon, Angew. Chemie Int. Ed. **46**, 4630 (2007).
[4] F. Wang, V. N. Richards, S. P. Shields, and W. E. Buhro, Chem. Mat. 2013 (advance article, volume and page not yet assigned DOI: 10.1021/cm402139r)
[5] F. S. Wilkinson, R. F. Norwood, J. M. McLellan, L. R. Lawson, and D. L. Patrick, J. Am. Chem. Soc. **128**, 16468 (2006).
[6] Y. Wu, and P. J. Yang, Am. Chem. Soc. **123**, 3165 (2001).
[7] J. W. Evans, P. A. Thiel, and M. C. Bartelt, Surf. Sci. Rep. **61**, 1 (2006).
[8] L. J. Lauhon, M. S. Gudiksen, and C. M. Lieber, Phil. Trans. R. Soc. Lond. A **362**, 1247 (2004).
[9] T. Sugimoto, Monodispersed Particles (Elsevier Science B.V.: Amsterdam, 2001).
[10] M. F. Casula, Y.-W Jun, D. J. Zazinsky, E. M. Chan, A. Corrias, and A. P. Alivisatos, J. Am. Chem. Soc. **128**, 1675 (2006).
[11] Y. Huang, and J. E. Pemberton, Colloid Surface A **360**, 175 (2010).
[12] M. Rahaman and M. N. Rahaman, Ceramic Processing p. 72 (CRC Press, Boca Raton, 2007)
[13] R. F. Strickland-Constable and R. E. A. Mason, Nature **197**, 897 (1963).
[14] T. P. Melia and W. P. Moffitt, Ind. Eng. Chem. Fund. **3**, 313 (1964).
[15] M. A. Watzky and R. G. Finke, J. Am. Chem. Soc. **119**, 10382 (1997).
[16] M. A. Watzky and R. G. Finke, Chem. Mater. **9**, 3083 (1997).
[17] V. K. LaMer, and R. H. J. Dinegar, Am. Chem. Soc. **72**, 4847 (1950); V. K. LaMer, Ind. Eng. Chem. **44**, 1270 (1952).
[18] S. P. Shields, V. N. Richards, and W. E. Buhro, Chem. Mater. **22**, 3112 (2010).
[19] J. E. Pemberton, and Y. Huang, Coll. Surf. A **360**, 175 (2010).
[20] D. T. Robb, and V. Privman, Langmuir **24**, 26 (2008).
[21] V. Privman, D. V. Goia, J. Park, and E. J. Matijevi, Coll. Interf. Sci. **213**, 36 (1999).
[22] It is likely that DBN, with its short transient nucleation regime, is dominated by ALA, although the distinction is not a necessary component of the current work; c.f. J.A. Venables and H. Brune, Phys. rev. B **66**, 195404 (2002).
[23] J. A. Venables, Philos. Mag. **27**, 697 (1973); J. A. Venables, and D. J. Ball, Proc. R. Soc. Lond. A **322**, 331 (1971).
[24] J. G. Amar, M. N. Popescu, and F. Family, Phys Rev. Lett. **86**, 3092 (2001); M. N. Popescu, J. G. Amar, F. Family, Phys. Rev. B **64**, 205404 (2001).
[25] M. C. Bartelt, and J. A. Evans, Phys. Rev. B **54**, 17359 (1996).
[26] For a review of the two-component MFRE approach, see A. L. Barabasi and H. E. Stanley, Fractal Concepts in Surface Growth; (Cambridge University Press: Cambridge, UK, 1995.)
[27] Although the proposed model is excellent for incorporating CNT drivers into the rate kinetics, the simplified two-component model does not allow for the prediction of crystal size distributions; this would require a full set of rate equations for each cluster size.
[28] J. W. Gibbs, The Collected Works of J. Willard Gibbs; (Yale Univ. Press: New Haven, 1948).
[29] S. L. Girshick and C.-P. Chiu, J. Chem. Phys. **93**, 1273 (1990).
[30] S. L. Girshick, J. Chem. Phys. 94, 826 (1991).
[31] The assumption of spherical clusters is made for simplicity; the important features of DBN produced by the model don't depend upon this assumption, and the inclusion of different geometries, growth habits, size-dependent surface energies, and dimensional scaling may be incorporated into the free energy.
[32] D. J. Walton, Chem. Phys. **37**, 2182 (1962).
[33] R. Z. Smoluchowski, Phys. Chem. **29**, 129 (1917).
[34] R.S. Wagner and W.C. Ellis, Appl. Phys. Let. **4**, 89 (1964).
[35] A.P. Levitt, Whisker Technology; (Wiley, New York, 1970).
[36] T.J. Trentler, K. M. Hickman, S.C. Goel, A.M. Viano, P.C. Gibbons, W.E. Buhro, Science **270**, 1791 (1995).
[37] A.M. Morales and C.M. Lieber, Science **279**, 208 (1998).
[38] M. Voigt, S. Dorsfield, A. Volz, and M. Sokolowski, Phys. Rev. Lett. **91**, 026103 (2003).
[39] X. Liu and M. Wuttig Phys. Rev. B **73**, 033405 (2006).
[40] T Shimada, Y. Ishii, K. Ueno and T. Hasegawa, J. Cryst. Growth **311**, 163 (2008).
[41] Y. Ishii, T. Shimada, N. Okazaki and T. Hasegawa, Langmuir **23**, 6864 (2007).
[42] Y. Takeyama, S. Maruyama and Y. Matsumoto, Cryst. Gr. Design **11**, 2273 (2011).
[43] Y. Takeyama, S. Ono and Y. Matsumoto, Appl. Phys.

Let. **101**, 083303 (2012).
[44] Y. Takeyama, S. Mantoku, S. Maruyama and Y. Matsumoto, CrystEngComm. **16**, 684 (2014).
[45] F.S. Wilkinson, R. F. Norwood, J.M. McLellan, L.R. Lawson and D.L. Patrick, J. Am. Chem. Soc. **128**, 16468 (2006).
[46] Samples involving pre-saturated solvent layers were formed by spin coating BES in which excess tetracene had been dissolved and allowed to equilibrate for several days.
[47] D. W. Shaw, K. Bufkin, A. A. Baronov, B. L. Johnson, and D. L. Patrick, J. Appl. Phys. **111**, 074907 (2012).
[48] The timescale for a molecule to diffuse the thickness of the solvent layer is $\approx 10^{-2}s$, much shorter than the timescale of the experiment.
[49] R. B. Campbell, J. M. Robertson, and J. Trotter, Acta Crystallogr. **15**, 289 (1962).
[50] J. Wansche, G. Tarabella, S. Bertolazzi, M. Bocoum, N. Copped, L. Barba, G. Arrighetti, L. Lutterotti, S. Iannotta, F. Cicoirae, and C. Santato, J. Mat. Chem. C **1**, 967 (2013).
[51] D. A. King and M. G. Wells, Proc. R. Soc. London **339**, 245 (1974).
[52] L. Yu, and P. Roco i Cabarrocas, Phys. Rev. B **80**, 085313 (2009).
[53] For an excellent review of mean crystal density scaling from rate equations, see ref 7, section 6.2.
[54] D. Kandel, Phys. Rev. Lett. **78**, 499 (1997).
[55] A detailed study of this result in conjunction with Monte Carlo simulations is under way.